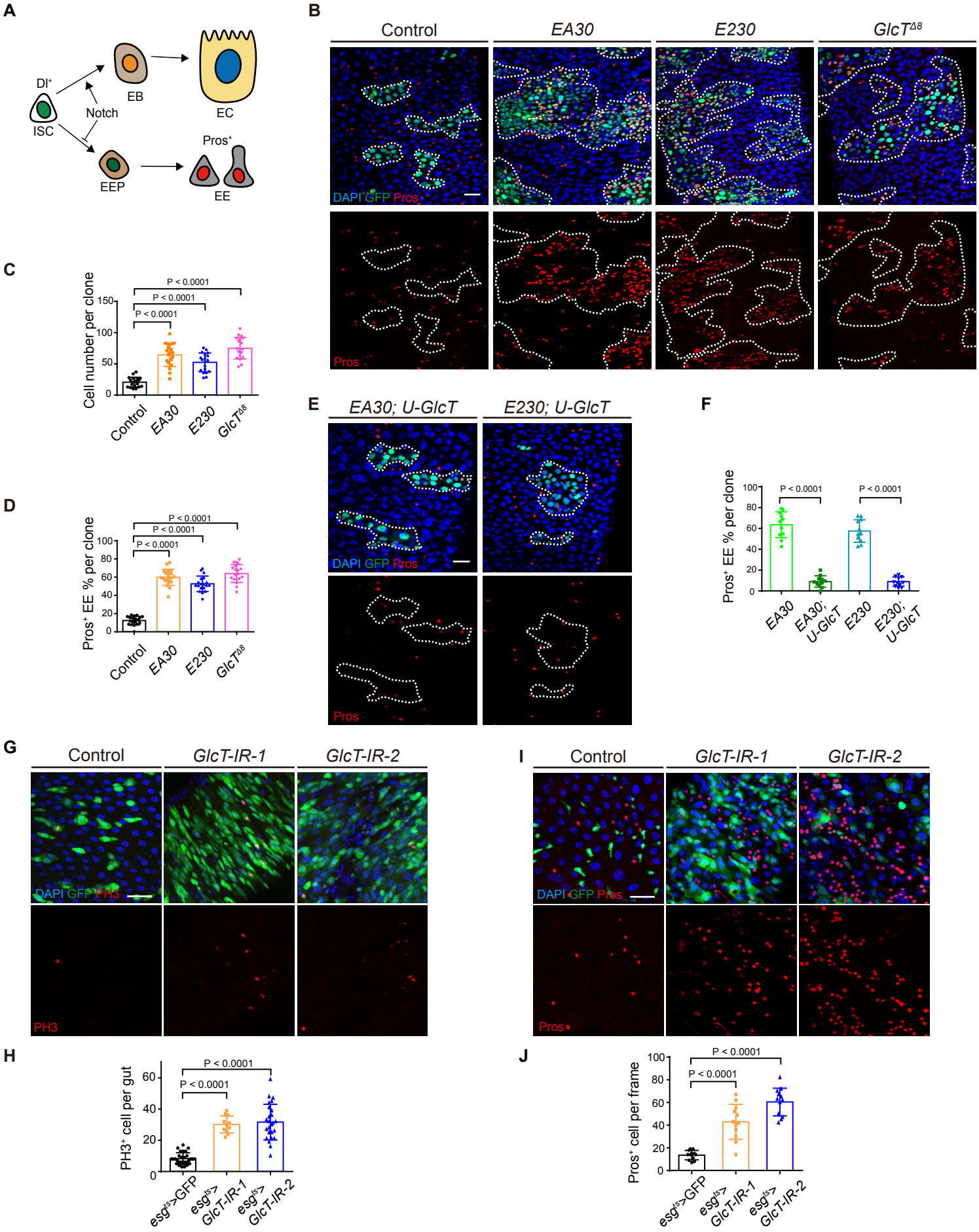
A
Dl+
ISC
Notch
EB
EC
EEP
Pros+
EE
B
Control
EA30
E230
GlcTΔ8
DAPI GFP Pros
Pros
C
Cell number per clone
P < 0.0001
P < 0.0001
P < 0.0001
Control
EA30
E230
GlcTΔ8
D
Pros+ EE % per clone
P < 0.0001
P < 0.0001
P < 0.0001
Control
EA30
E230
GlcTΔ8
E
EA30; U-GlcT
E230; U-GlcT
DAPI GFP Pros
Pros
F
Pros+ EE % per clone
P < 0.0001
P < 0.0001
EA30
EA30; U-GlcT
E230
E230; U-GlcT
G
Control
GlcT-IR-1
GlcT-IR-2
DAPI GFP PH3
PH3
H
PH3+ cell per gut
P < 0.0001
P < 0.0001
esgts>GFP
esgts> GlcT-IR-1
esgts> GlcT-IR-2
I
Control
GlcT-IR-1
GlcT-IR-2
DAPI GFP Pros
Pros
J
Pros+ cell per frame
P < 0.0001
P < 0.0001
esgts>GFP
esgts> GlcT-IR-1
esgts> GlcT-IR-2

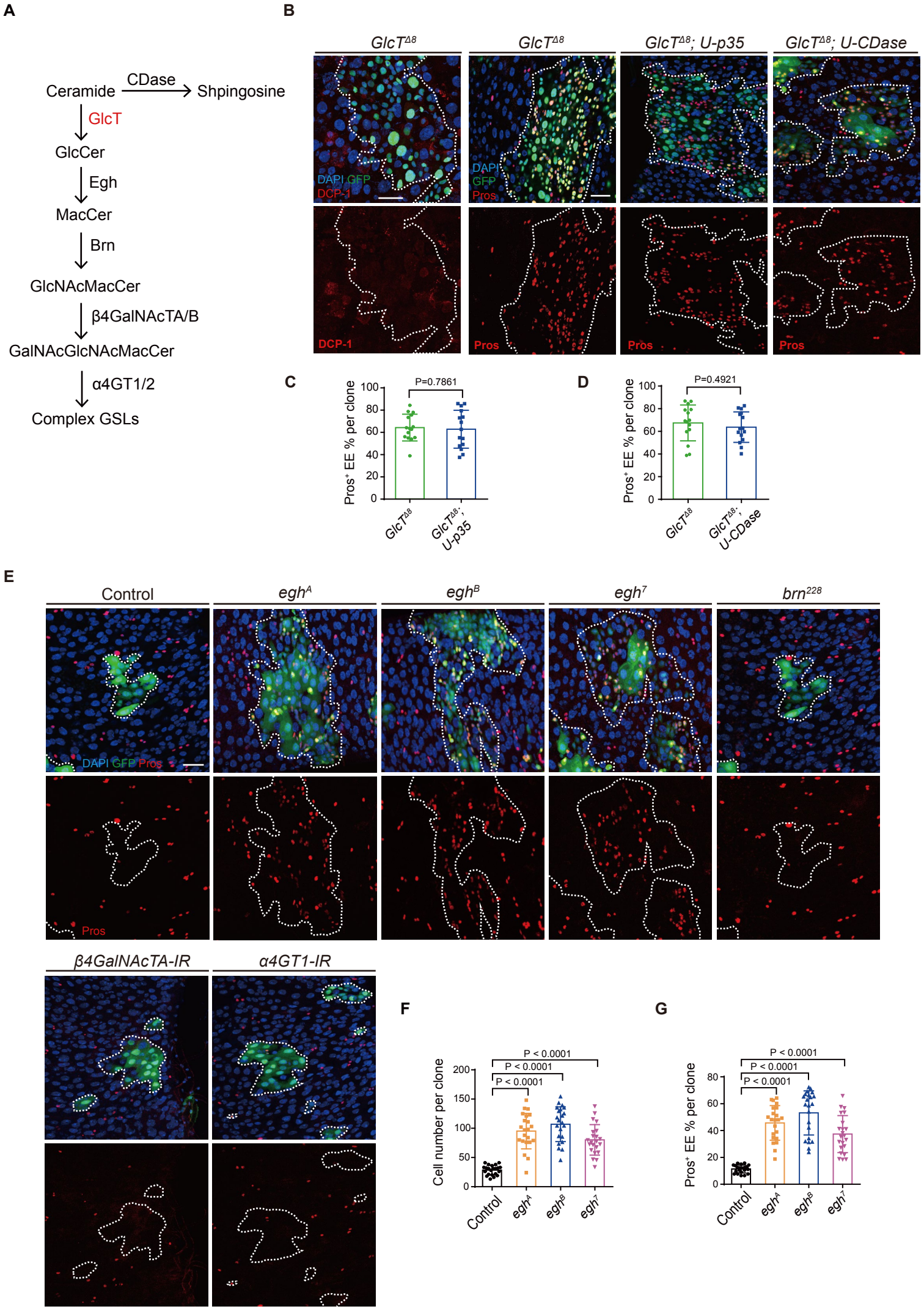
A
Ceramide
CDase
Shpingosine
GlcT
GlcCer
Egh
MacCer
Brn
GlcNAcMacCer
β4GalNAcTA/B
GalNAcGlcNAcMacCer
α4GT1/2
Complex GSLs
B
GlcTΔ8
GlcTΔ8
GlcTΔ8; U-p35
GlcTΔ8; U-CDase
DAPI GFP
DCP-1
DAPI
GFP
Pros
DCP-1
Pros
Pros
Pros
C
P=0.7861
Pros+ EE % per clone
GlcTΔ8
GlcTΔ8; U-p35
D
P=0.4921
Pros+ EE % per clone
GlcTΔ8
GlcTΔ8; U-CDase
E
Control
eghA
eghB
egh7
brn228
DAPI GFP Pros
Pros
β4GalNAcTA-IR
α4GT1-IR
F
P < 0.0001
P < 0.0001
P < 0.0001
Cell number per clone
Control
eghA
eghB
egh7
G
P < 0.0001
P < 0.0001
P < 0.0001
Pros+ EE % per clone
Control
eghA
eghB
egh7

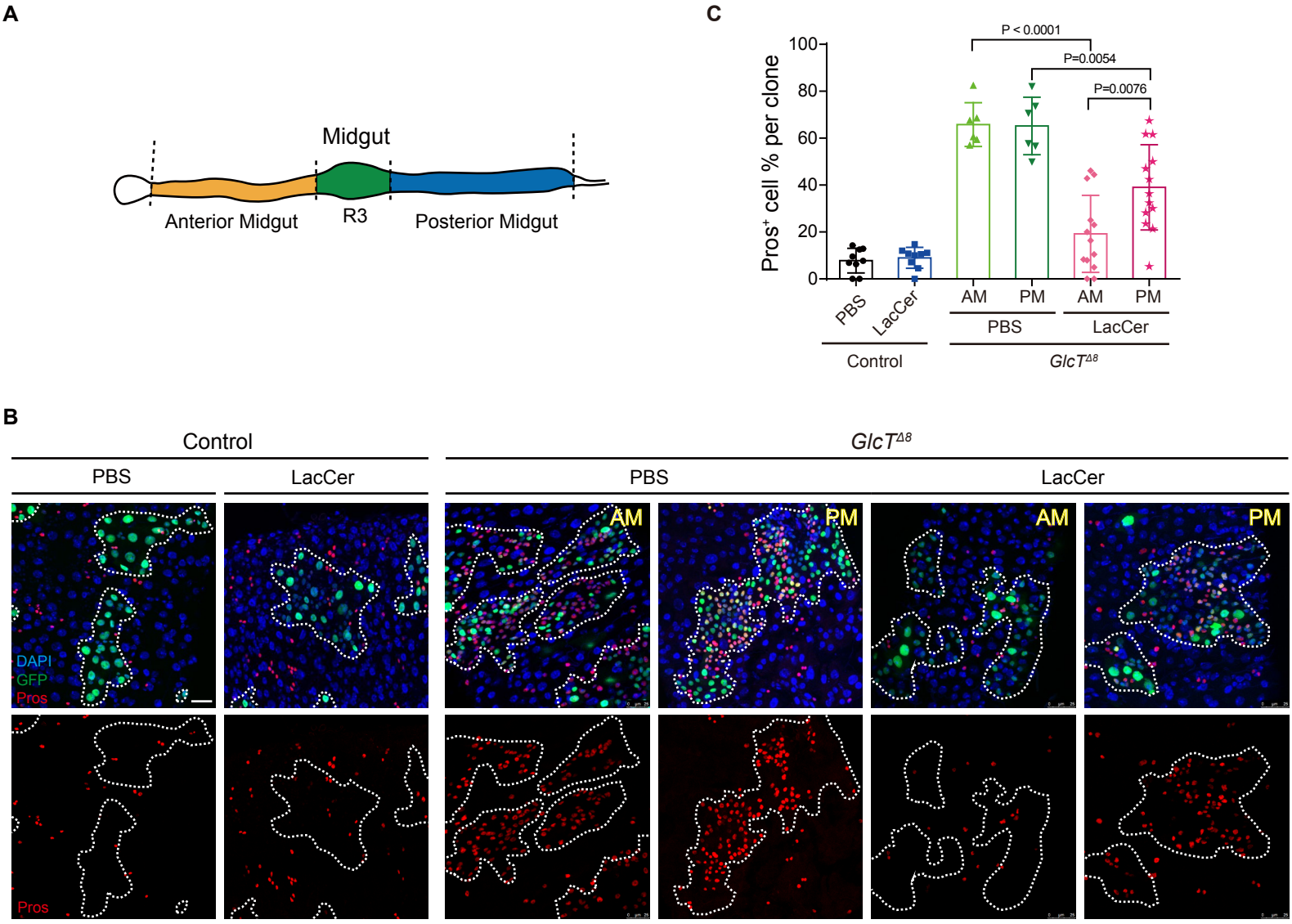
A
Midgut
Anterior Midgut
R3
Posterior Midgut
C
Pros+ cell % per clone
100
80
60
40
20
0
P < 0.0001
P=0.0054
P=0.0076
PBS
LacCer
AM
PM
AM
PM
PBS
LacCer
Control
GlcTΔ8
B
Control
GlcTΔ8
PBS
LacCer
PBS
LacCer
AM
PM
AM
PM
DAPI
GFP
Pros
Pros

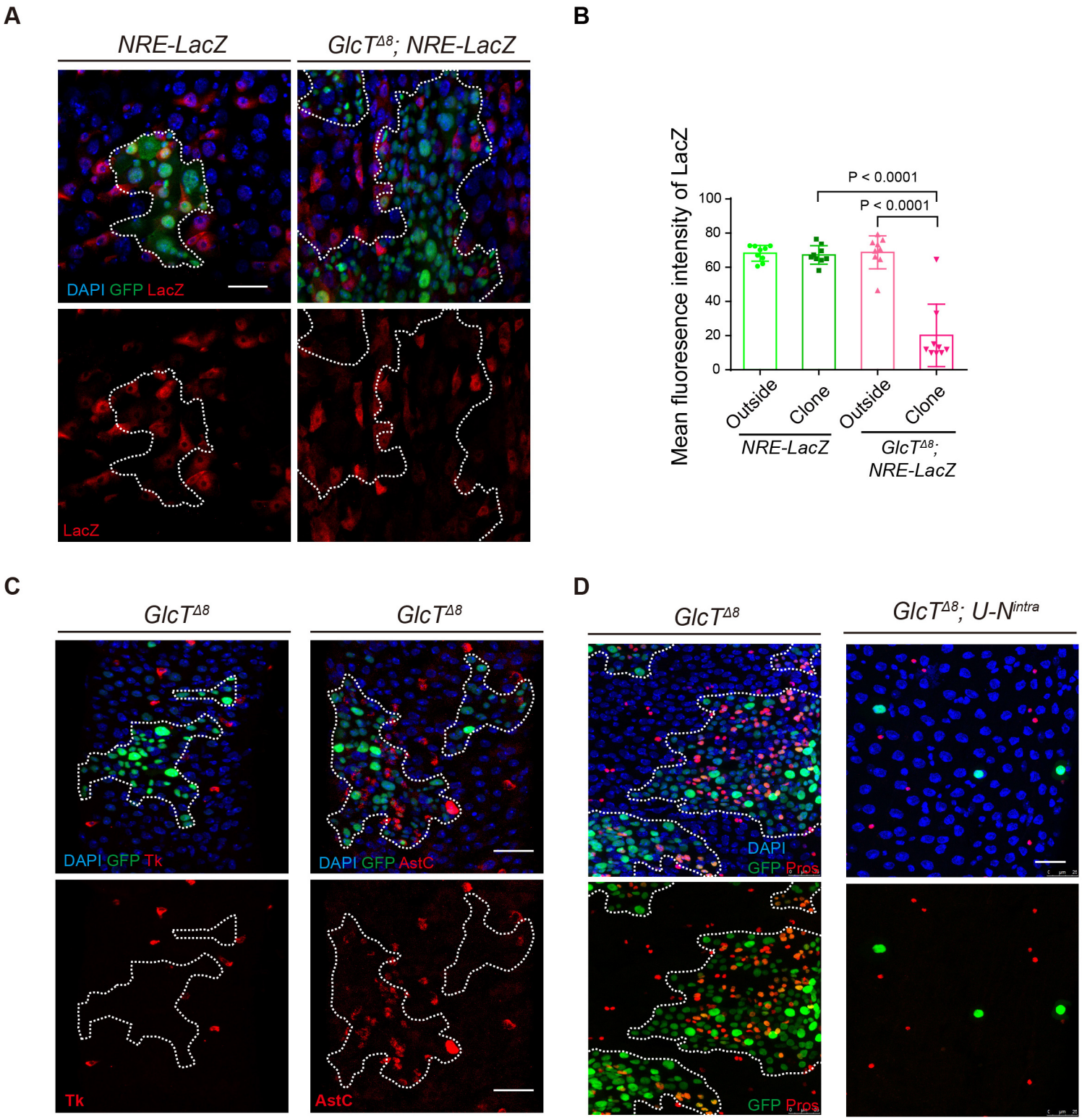
A
NRE-LacZ
GlcT$^{\Delta 8}$; NRE-LacZ
DAPI GFP LacZ
LacZ
B
Mean fluorescence intensity of LacZ
P < 0.0001
P < 0.0001
100
80
60
40
20
0
Outside
Clone
Outside
Clone
NRE-LacZ
GlcT$^{\Delta 8}$; NRE-LacZ
C
GlcT$^{\Delta 8}$
GlcT$^{\Delta 8}$
DAPI GFP Tk
DAPI GFP AstC
Tk
AstC
D
GlcT$^{\Delta 8}$
GlcT$^{\Delta 8}$; U-N^{intra}
DAPI
GFP Pros
GFP Pros

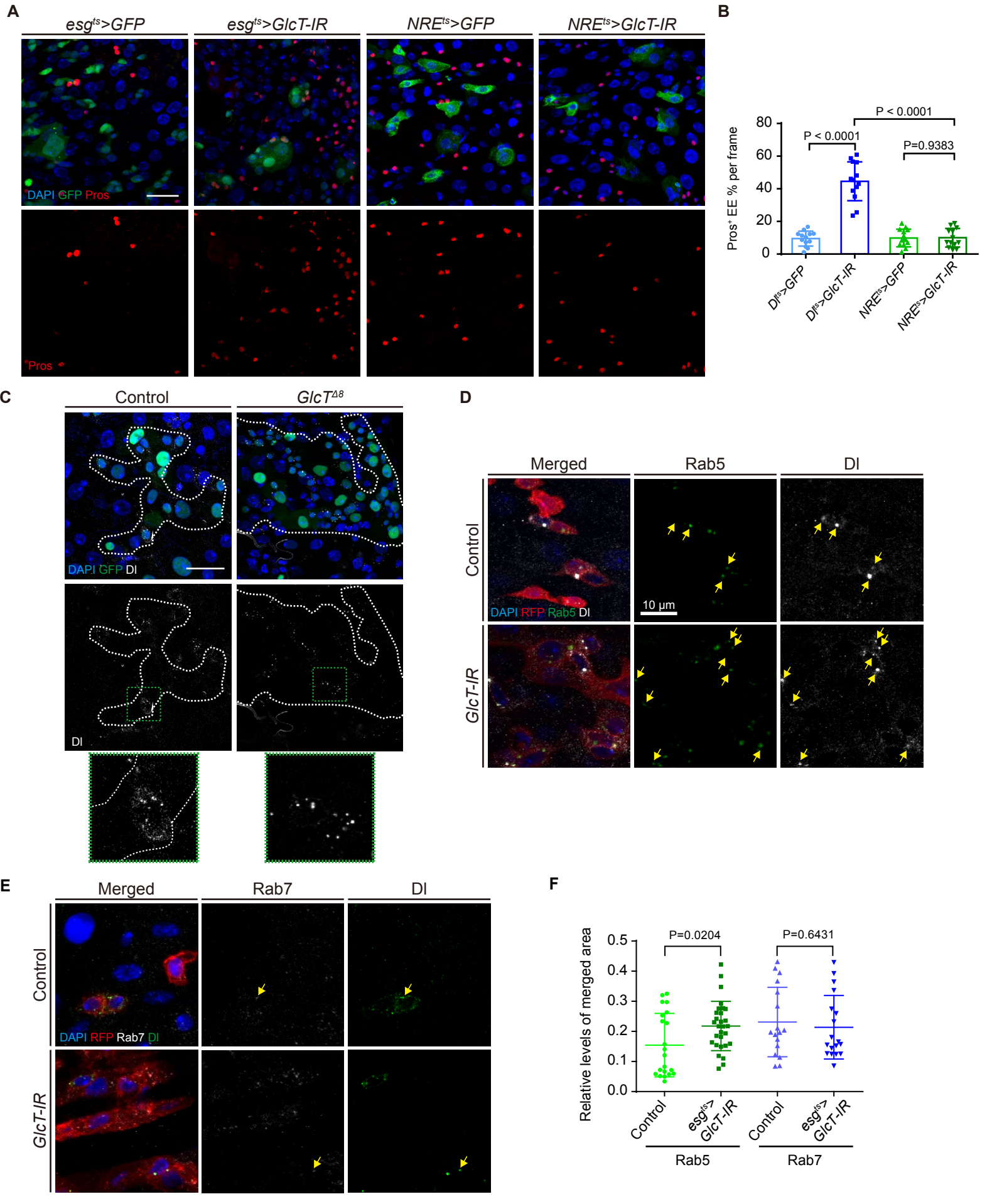
A
esg^ts>GFP
esg^ts>GlcT-IR
NRE^ts>GFP
NRE^ts>GlcT-IR
DAPI GFP Pros
Pros
B
Pros+ EE % per frame
80
60
40
20
0
P < 0.0001
P < 0.0001
P=0.9383
Dl^ts>GFP
Dl^ts>GlcT-IR
NRE^ts>GFP
NRE^ts>GlcT-IR
C
Control
GlcT^Δ8
DAPI GFP Dl
Dl
D
Merged
Rab5
Dl
Control
GlcT-IR
DAPI RFP Rab5 Dl
10 μm
E
Merged
Rab7
Dl
Control
GlcT-IR
DAPI RFP Rab7 Dl
F
Relative levels of merged area
0.5
0.4
0.3
0.2
0.1
0.0
P=0.0204
P=0.6431
Control
esg^ts> GlcT-IR
Control
esg^ts> GlcT-IR
Rab5
Rab7

A

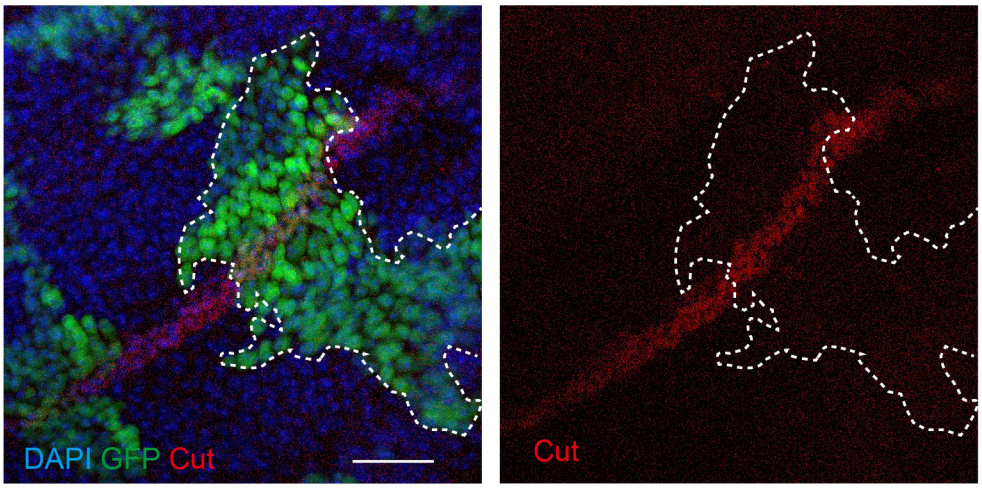

B

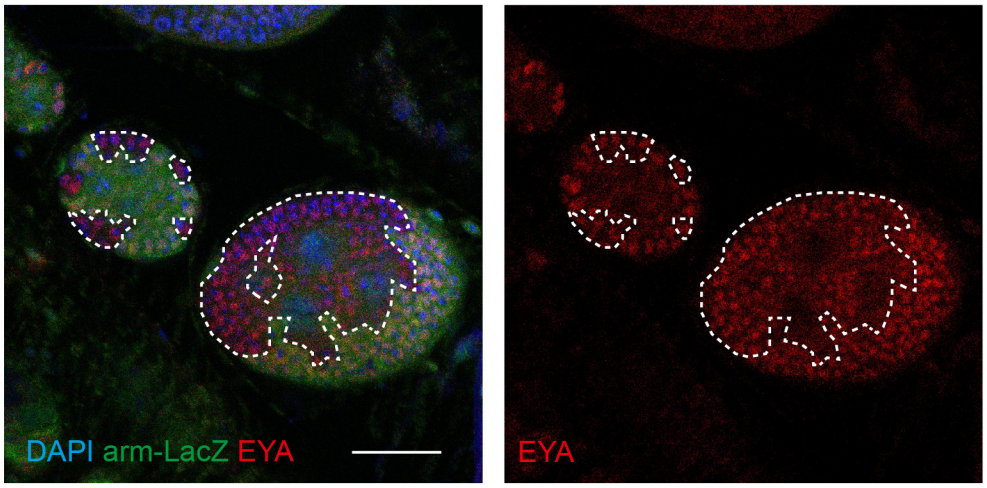

C

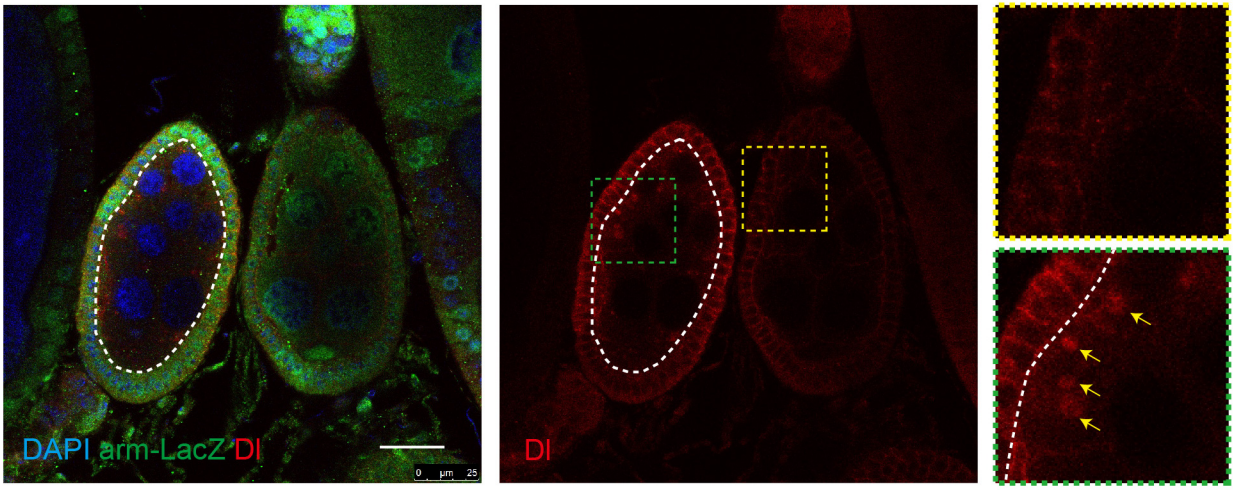

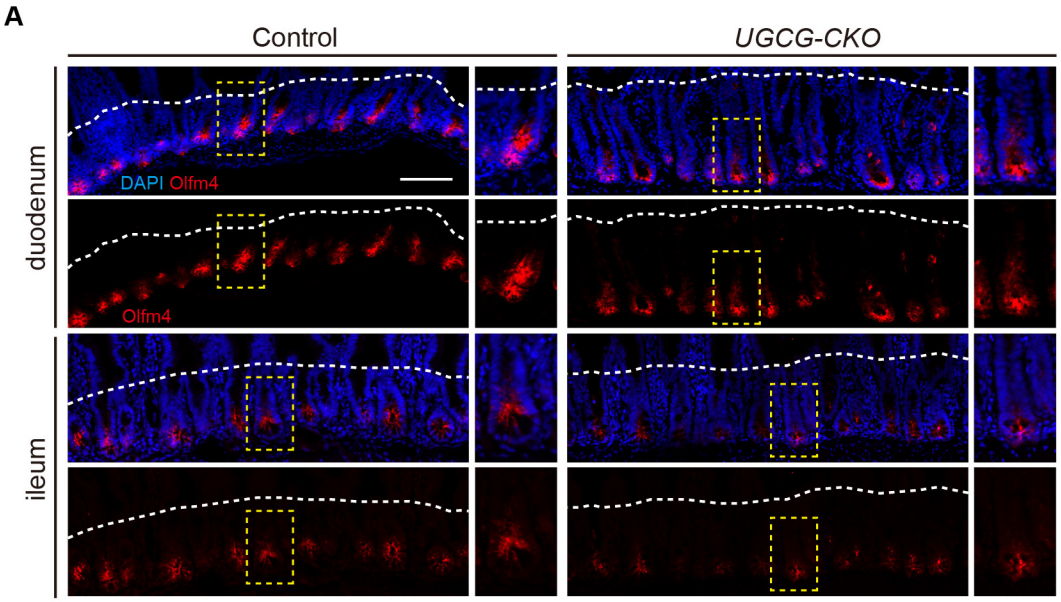
A
Control
UGCG-CKO
duodenum
ileum
DAPI Olfm4
Olfm4

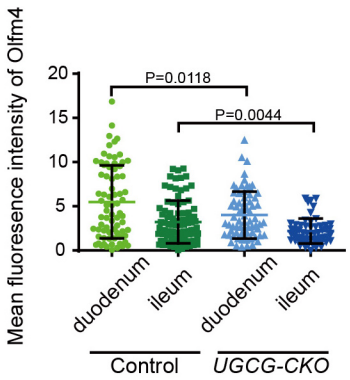
B
Mean fluoresence intensity of Olfm4
20
15
10
5
0
P=0.0118
P=0.0044
duodenum
ileum
duodenum
ileum
Control
UGCG-CKO

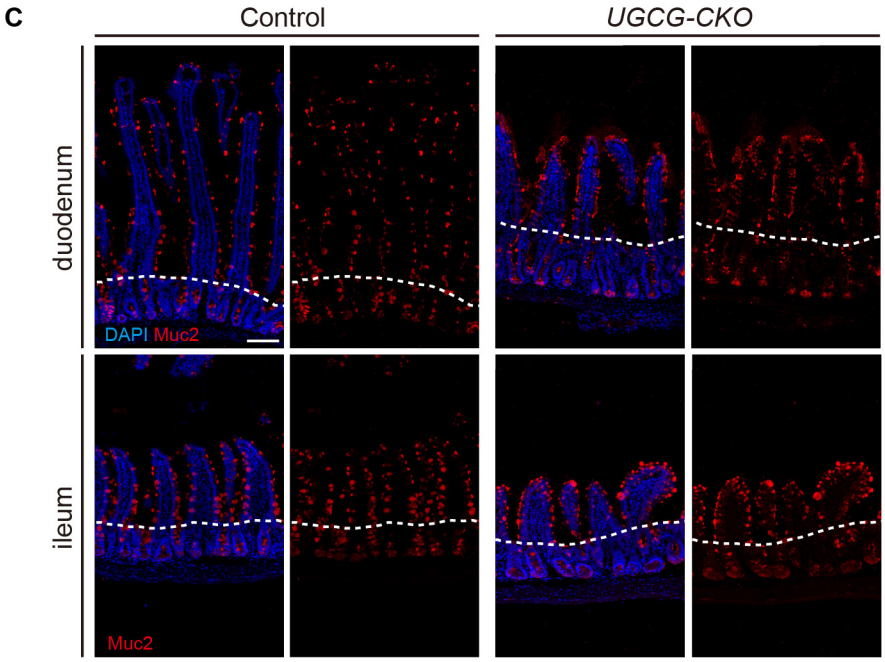
C
Control
UGCG-CKO
duodenum
ileum
DAPI Muc2
Muc2

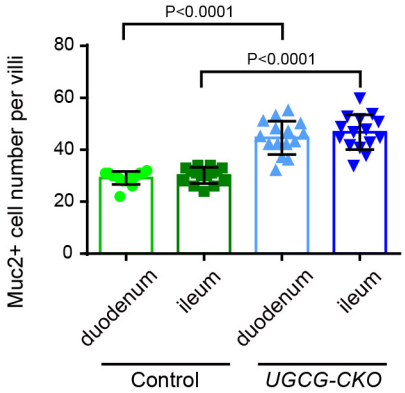
D
Muc2+ cell number per villi
80
60
40
20
0
P<0.0001
P<0.0001
duodenum
ileum
duodenum
ileum
Control
UGCG-CKO

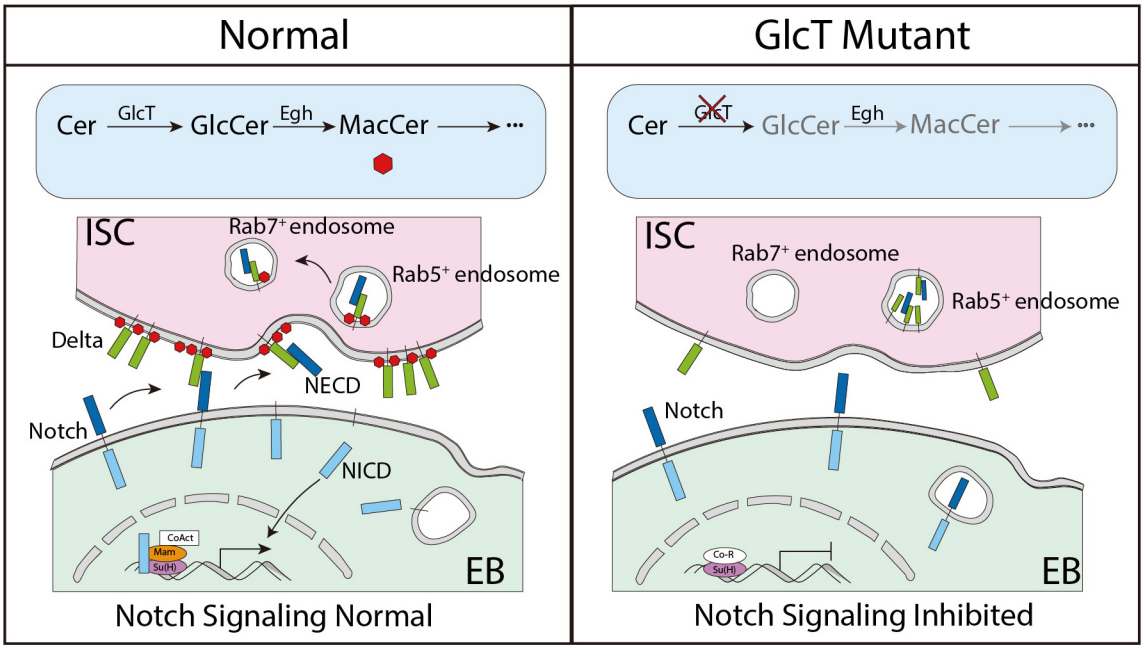
E
Normal
GlcT Mutant
Cer
GlcT
GlcCer
Egh
MacCer
ISC
Rab7⁺ endosome
Rab5⁺ endosome
Delta
NECD
Notch
NICD
CoAct
Mam
Su(H)
EB
Notch Signaling Normal
Co-R
Notch Signaling Inhibited

Mac/Lac-tosylceramide regulates intestinal homeostasis and secretory cell fate commitment by facilitating Notch signaling

Kebei Tang[1, 2#], Xuewen Li[1#], Jiulong Hu[1, 3#], Jingyuan Shi[1], Yumei Li[1], Yansu Chen[1], Chang Yin[1], Fengchao Wang[1, 4], and Rongwen Xi[1, 4*]

[1] National Institute of Biological Sciences, No. 7 Science Park Road, Zhongguancun Life Science Park, Beijing 102206, China

[2] Academy for Advanced Interdisciplinary Studies, Peking University, Beijing 100871, China

[3] School of Life Sciences, Tsinghua University, Beijing 100084, China

[4] Tsinghua Institute of Multidisciplinary Biomedical Research, Tsinghua University, Beijing 102206, China.

[#] These authors contributed equally to this work.

* Correspondence: *xirongwen@nibs.ac.cn*

Abstract

Cell-to-cell communication via Delta-Notch signaling is widely used in various tissues and organs to regulate development and patterning; however, the mechanisms regulating Notch signaling for precise cell fate decisions remain poorly understood. Similar to mammals, the intestinal stem cells (ISCs) in the adult *Drosophila* midgut generate both absorptive and secretory cell progeny, guided by differential levels of Notch activation. Here we performed a forward genetic screen in *Drosophila* and identified glucosylceramide synthase (GlcT), a rate-limiting enzyme for glycosphingolipid (GSL) production, whose mutation causes the development of secretory cell tumors. Genetic analysis of the GSL synthesis pathway, combined with metabolite rescue experiments, revealed that the tumor formation is linked to a deficiency in Mactosylceramide/Lactosylceramide. This deficiency impaired the endocytic recycling of the Delta, subsequently reducing Notch signaling activation. Conditional knockout of *UGCG*, the mammalian ortholog of *GlcT*, in mouse small intestine caused an excessive differentiation of goblet cells, phenotypes similar to these caused by Notch inhibition. Our study suggests an evolutionarily conserved role for a specific GSL metabolite in modulating Notch signaling during stem cell fate decisions and provides a molecular connection between ceramide metabolism and Notch signaling in regulating tissue homeostasis and tumor formation.

INTRODUCTION

Notch signaling is an evolutionarily conserved pathway in metazoans that mediates local cell-cell interactions through the membrane-tethered ligand Delta (Dl) and the membrane receptor Notch. This pathway transduces signals from the cell surface to the nucleus, regulating the transcription of target genes [1,2]. Dl-Notch signaling controls various cell fates and developmental processes, with mutations in the pathway implicated in numerous human diseases, including congenital defects and cancer [3-5]. Given that Notch can transduce, amplify, and consolidate molecular differences to influence cell fate decisions, it is crucial to understand how the strength of the Notch signaling pathway is precisely regulated to ensure proper cell fate determination and tissue development.

Notch signaling is known as a major regulator of cell fate decisions in both mammalian and *Drosophila* intestinal stem cell (ISC) lineages, as its activity determines the binary fate of intestinal progenitor cells. A high level of Notch activity promotes the specification of absorptive enterocytes, while low or absent Notch activity favors the specification of secretory cell types.[6,7]. The *Drosophila* intestinal stem cell (ISC) lineage in the adult midgut is relatively simple, comprising only one type of secretory cell: enteroendocrine cells (EEs). This simplicity makes it an attractive experimental system for studying Notch signaling in cell fate decisions during epithelial renewal [6]. The fly ISCs, which specifically express Dl, periodically generate two types of committed daughter cells: enteroblasts, which experience high levels of Notch activation and are primed for the specification of absorptive enterocytes, and enteroendocrine progenitor cells (EEPs), which receive low levels of Notch activation. Typically, EEPs undergo one round of mitosis before terminal differentiation, resulting in the formation of EE pairs [8-11]. The loss of Notch signaling results in a complete blockage of enteroblast differentiation, leading to the accumulation of ISCs, EEPs and EEs in the intestinal epithelium, producing an “EE tumor” phenotype [8,10]. It is suggested that the expression level of Dl in individual ISCs varies, leading to differential levels of Notch activation in the immediate daughter cells [9]. This variation in Dl expression may result from dynamic bidirectional Dl-Notch signaling between ISCs and EEPs, which in parallel or in conjunction

with an intrinsic feedback mechanism in ISCs, guides a periodic activation of an EE fate inducer Scute, thereby periodic generation of EEPs from ISCs [10,12,13]. The transient activation of Scute induces irreversible Prospero expression in EEPs through a Phyl-Sina-Ttk69 regulatory cascade, initiating terminal differentiation into EEs [10,14-16]. During the period of Scute inactivation, ISCs only generate enterocyte-committed enterobalsts by default via Dl-Notch mediated lateral inhibition [8,17]. In newly enclosed flies, increased lipid intake from food can alter the membrane trafficking of Dl, subsequently increasing the frequency of EE specification from ISCs [18]. Thus, both intrinsic and extrinsic mechanisms are involved in regulating Dl-Notch signaling to orchestrate stem cell fate decisions.

To better understand fate regulation in the *Drosophila* ISC lineage, here we conducted a forward mosaic genetic screen in the adult *Drosophila* midgut, focusing on the right arm of the second chromosome to identify genes whose mutations could disrupt ISC fate decisions. From this screen, we identified several complementation groups that result in EE tumor phenotypes. While most of the identified gene loci correspond to known components of the Notch signaling pathway, we discovered one gene locus not previously associated with Notch signaling. Further analyses revealed a specific GSL metabolite that regulates Notch signaling and cell fate decisions in the intestinal epithelium, and this function appears to be conserved from *Drosophila* to mice.

RESULTS

A mosaic genetic screen identifies *GlcT* as a tumor suppressor in the adult *Drosophila* midgut

We performed chemical mutagenesis on chromosome 2R (carrying FRTG13/42B) and used the MARCM system to induce mutant clones in the adult midgut (Supplementary Figure 1). We screened approximately 10,000 lethal lines and identified totally 12 mutations across six complementation groups that exhibited a "small cell tumor" phenotype, characterized by a significant accumulation of diploid cells within the clones (Supplementary Figure 1 and

94 supplementary Table 1). Co-staining with the ISC marker Dl and the EE cell marker Pros
95 revealed that most of these tumors contained an excessive number of ISCs and EEs, the EE
96 tumor phenotype commonly observed in Notch mutant clones [11,19]. Further genetic mapping
97 showed that three complementation groups were associated with genes known to function
98 in the Notch pathway: *mam*, *Gmer*, and *O-fut1* [20-22]. One complementation group, comprising
99 two alleles (*EA30* and *E230*), mapped to the *GlcT* gene (see details in Methods), while the
100 remaining two complementation groups, each consisting of one allele, remain undetermined
101 (Supplementary Table 1). *GlcT* encodes glucosylceramide synthase, an enzyme that catalyzes
102 the formation of glucosylceramide, the core component of glycosphingolipids (GSLs). Both
103 alleles carried one or more missense mutations resulting in the amino acid replacements
104 E292K (for *EA30*) and L395P/S397T (for *E230*, Figure S1D). The two mutations produced a
105 similar tumor phenotype in terms of tumor size and the composition of EEs in the tumors
106 (Figure 1B-D). The large polyploid cells were still present in the tumors, indicating that the
107 multipotency of ISCs was retained, but the differentiation of ISCs may have been biased
108 towards the EE fate commitment. Additionally, $GlcT^{\Delta 8}$, a previously characterized null allele of
109 *GlcT* [23], exhibited a similar EE tumor phenotype (Figure 1B-D). Expressing a *UAS-GlcT*
110 transgene in the mutant clones fully prevented the tumor phenotype (Figure 1E, F).
111 Furthermore, depleting *GlcT* in progenitor cells using RNAi with $esg\text{-}GAL4^{ts}$ also led to
112 overproliferation of ISCs and excessive generation of EEs in the midgut epithelium (Figure
113 1G-I). Taken together, these data suggest that *GlcT* acts as a tumor suppressor in adult
114 *Drosophila* midgut. Loss of *GlcT* induces ISC over-proliferation and excessive EE
115 differentiation, resulting in an EE tumor or "neuroendocrine tumor (NET)" phenotype.

116

117 **Genetic analysis of the GSL synthesis pathway components reveals specific**
118 **tumor-suppressive activity for *egh*, in addition to *GlcT***

119 GlcT is involved in the initial step in the GSL biosynthesis pathway, which synthesizes
120 glucosylceramide by transferring glucose to ceramide (Figure 2A). The loss of *GlcT* could
121 result in the accumulation of ceramide or the absence of glucosylceramide and the
122 downstream GSL metabolites. Ceramide accumulation has been linked to promoting cell

apoptosis [24], which could potentially explain the ISC over-proliferation phenotype since apoptotic cells can induce compensatory ISC proliferation [25]. However, we did not observe a significant increase in apoptotic cells within the mutant clones (Figure 2B). Moreover, the overexpression of p35, an inhibitor of cell apoptosis, failed to suppress or alleviate the tumor phenotype (Figure 2B). Ceramidase (CDase) catalyzes ceramide into shingosine and free fatty acid, and overexpressing *CDase* can in theory downregulate ceramide levels. We therefore introduced *CDase* expression in the mutant clones, but this intervention also did not alleviate the tumor phenotype (Figure 2B). Hence, the EE tumors developed from *GlcT* mutant clones is unlikely caused by the accumulation of ceramide.

In the GSL biosynthesis pathway in *Drosophila*, glucosylceramide undergoes sequential modifications catalyzed by Egghead (Egh) and Brainiac (Brn), which add the second (Mactosyl-) and third (GlcNAc-) glycosyl residues, respectively (Figure 2A) [26,27]. This leads to the synthesis of Mactosylceramide (MacCer) and GlcNAcβ1-3Manβ1-4Glcβ1Ceramide. Complex GSL biosynthesis involves the participation of β4-N-Acetylgalactosyltransferase (*β4GalNAcTA/TB*) and α1,4-Galactosyltransferase (*α4GT1/2*) in the fourth and fifth steps of GSL sugar chain elongation [28,29]. These enzymes catalyze the formation of GalNAcβ1-4GlcNAcβ1-3Manβ1-4Glcβ1Ceramide and GalNAc-α1-4GalNAcβ1-4GlcNAcβ1-3Manβ1-4Glcβ1Ceramide, respectively.

To understand the consequences of mutations in these GSL biosynthesis pathway genes, we generated mutant MARCM clones for each of the above-mentioned genes and examined their effects. Interestingly, mutations in *egh*, assessed using three different loss-of-function alleles, consistently resulted in cell over-proliferation and excessive EE phenotypes, similar to those caused by the loss of *GlcT* (Figure 2E-G). In contrast, none of the mutant clones of *brn*, *β4GalNAcTA*, or *α4GT1* exhibited any noticeable abnormalities in clone size or percentages of EEs, when compared to the control group of wild-type clones (Figure 2E-G). Therefore, GlcT and Egh, but not other enzymes in the GSL biosynthesis pathway, exhibit specific tumor

151 suppressive activity in the adult *Drosophila* midgut.

152

153 **The EEC tumor phenotype is a result of MacCer deficiency**

154 As Egh is necessary for the biosynthesis of MacCer, the specific phenotype resulted from the
155 loss GlcT and Egh but not Brn could be attributed to the absence of MacCer. To test this
156 hypothesis, we fed flies carrying *GlcT* mutant clones with Lactosylceramide (LacCer), an
157 analog of MacCer that functions similarly to MacCer in mammalian cells. Remarkably, LacCer
158 significantly suppressed the overgrowth and excessive EE phenotype in the anterior midgut
159 clones (Figure 3B, C). The suppression effect was also significant, though relatively mild, in
160 the posterior midgut (Figure 3B, C). This difference may be attributed to substantial
161 absorption or metabolism of LacCer prior to its entry into the posterior midgut. Therefore,
162 among the various GSL metabolites, MacCer and LacCer appear to possess specific
163 tumor-suppressive activities in the *Drosophila* midgut.

164

165 **Loss of *GlcT* leads to reduced activation of Notch signaling in ISC progenies.**

166 In adult *Drosophila* midgut, the proliferation and differentiation of ISCs are regulated by
167 multiple signaling pathways. Among these, the EGFR/Ras/MAPK and JAK/STAT signaling
168 pathways play significant roles in promoting ISC proliferation during intestinal renewal and
169 regeneration following tissue damage or infection [30,31]. Additionally, Notch signaling not only
170 regulates ISC proliferation but also controls fate decisions between EE/EC during ISC
171 differentiation [19,32,33]. Loss of Notch leads to increased ISC proliferation and excessive EE
172 generation, phenotype similar to those caused by *GlcT* mutations. Therefore, we examined
173 whether the loss of *GlcT* affects the activities of these signaling pathways.

174

175 Normally, among the intestinal cells in the midgut epithelium, progenitor cells including ISCs
176 and enteroblasts, exhibit low but specific activation of EGFR and JAK/STAT activities [30,31,34].
177 The growth of *GlcT* mutant clones appeared to cause a general increase of EGFR and

178 JAK/STAT activities within the intestinal epithelium, as many differentiated cells also
179 exhibited EGFR or JAK/STAT signaling activation (Supplementary Figure 2), which is likely due
180 to stress responses induced by tumor growth [35]. Nevertheless, we observed that pERK, a
181 direct indicator of EGFR/Ras/MAPK signaling activity, was not significantly increased in *GlcT*
182 mutant cells compared to cells outside the clones (Supplementary Figure 2). Similarly, the
183 nuclear expression of STAT92E, which reflects JAK/STAT pathway activation, did not show
184 significant changes in *GlcT* mutant cells compared to normal cells outside the clones
185 (Supplementary Figure 2). However, the expression of *NRE-lacZ*, a reporter for Notch
186 pathway activation, was specifically down-regulated in *GlcT* mutant clones. Most cells within
187 the clones exhibited lower LacZ expression levels compared to *NRE-lacZ* positive cells outside
188 the clones (Figure 4A, B). Previous studies have shown that while the loss of function of
189 Notch completely blocks EC differentiation from ISCs, a reduction in Notch activity does not
190 necessarily hinder EC differentiation from ISCs. Instead, it may lead to a dose-dependent
191 increase in the ratio of differentiated EEs to ECs, depending on the severity of Notch loss [19].
192 Therefore, the increased EE to EC ratio and the reduced NRE-lacZ expression observed in
193 *GlcT* mutant clones collectively suggest that the mutant phenotype may be caused by a
194 reduction in Notch signaling activity.

195

196 In the ISC lineage, Notch signaling not only guides EC/EE fate decisions, but is also
197 participated in regulating EE subtype diversity. Typically, each EEP undergo one round of
198 asymmetric cell division to yield a pair of distinctive EEs, an allatostatin C $(AstC)^+$ class I EE
199 and a tachykinin $(Tk)^+$ class II EE [10]. The loss of *Notch* specifically compromises
200 Mirr-dependent specification of class II EE generation, resulting in all EEs in *Notch* mutant
201 clones becoming $AstC^+$ class I EEs [16,36]. We found that in *GlcT* mutant clones, virtually all EEs
202 were positive for AstC but TK (Figure 4C), further supporting the idea that Notch signaling is
203 compromised in these clones.

204

205 We next tested whether forced activation of Notch in *GlcT* mutant clones could suppress the

206 EE tumor phenotype. To achieve this, we expressed N^{intra}, an active form of Notch, in *GlcT*
207 mutant clones. As expected, this resulted in the complete suppression of cell proliferation in
208 *GlcT* mutant clones and promoted the differentiation of these cells into ECs, leading all
209 clones to become single-cell clones that often contained a polyploid cell (Figure 4D). This
210 finding suggests that N^{intra} is epistatic to *GlcT* in the signaling transduction pathway,
211 indicating that GlcT may regulate Notch signaling at the ligand/receptor level.

212

213 ***GlcT* regulates the endocytic trafficking of Delta.**

214 The observations above collectively suggest that full activation of Notch signaling in the ISC
215 lineage may require a specific GSL: Mac/Lac-Cer. As transmembrane proteins, the proper
216 internalization and recycling of Dl and Notch are important for the proper activation of Notch
217 signaling [37,38]. Specific lipids have been implicated in the formation of micro-domains on the
218 cell membrane, which play a role in regulating cell-cell signaling [39]. Therefore, we asked
219 whether the loss of MacCer caused by *GlcT* mutation could disrupt Notch signaling by
220 affecting the stability, endocytosis, or recycling of either Dl or Notch.

221

222 Knocking down *GlcT* in ISCs using *Dl-GAL4*^{ts} cased an increase in EEs in the midgut epithelium
223 (Figure 5 A, B). However, when *GlcT* was specifically knocked down in EBs using *NRE-GAL4*^{ts},
224 there was no noticeable increase in EEs (Figure 5 A, B). This suggests that *GlcT* is specifically
225 required in ISCs and implies its potential role on the regulation of Dl. It is well-known that
226 the internalization of Dl in the signaling-sending cell is necessary for Notch activation in the
227 signaling-receiving cell [37]. To investigate whether the endocytosis process of Dl is altered in
228 *GlcT* mutant ISCs, we performed an *ex vivo* Dl internalization assay, following the previously
229 described protocol [40]. In this assay, we cultured and incubated the freshly dissected gut with
230 anti-Dl antibodies, and the endocytosis of the antibody-labeled Dl was visualized after
231 fixation and immunostaining with secondary antibodies. Interestingly, during the 3-hour
232 period, we observed a significant difference in the subcellular localization pattern of Dl
233 between normal and *GlcT* mutant ISCs (Figure 5 C). In *GlcT* mutant ISCs, the majority of

234 labeled Dl had already been internalized, while in wild-type ISCs, it remained on the cell
235 membrane. This observation suggests that the loss of *GlcT* causes either reduced stability of
236 Dl on the cell membrane or accelerated internalization of Dl from the cell membrane.

237

238 To further characterize the endocytic trafficking of Dl in *GlcT* mutant ISCs, we performed
239 conditional depletion of *GlcT* and examined the co-localization of internalized Dl with the
240 early endosome marker Rab5 and the late endosome marker Rab7, respectively. In
241 comparison to control ISCs, *GlcT-RNAi* ISCs exhibited a significant increase in early
242 endosomes containing Dl (Figure 5D, F). However, the percentage of late endosomes
243 containing Dl remained similar between wild-type and *GlcT-RNAi* ISCs (Figure 5E, F). These
244 observations suggest that the internalized Dl in *GlcT-RNAi* ISCs experiences a delay in early
245 endosomes, which might cause a delay in Dl recycling and consequently a reduction in
246 Dl-Notch signaling activity (Figure 7E).

247

248 ***GlcT* shows tissue specificity in regulating Notch signaling activity**

249 Notch signaling has pleiotropic function and is known to be participated in the development
250 of diverse tissue and organs. We therefore asked whether the discovered mechanism above
251 is generally utilized in controlling Notch signaling in diverse tissues and organs. In the wing
252 disc of third instar larvae, Notch signaling is activated by ligands Dl and Serrate at the
253 dorsal-ventral boundary to induce the expression of Cut [41]. We found that in *GlcT* mutant
254 clones spanning the dorsal-ventral boundary region of the wing disc, the expression of Cut
255 was not significantly altered (Figure 6A). This indicates that *GlcT* is not essential for
256 regulating Notch-mediated Cut expression in this specific context.

257

258 During oogenesis in the *Drosophila* ovary, Notch signaling regulates differentiation and
259 transition of follicle cells from the mitotic cell cycle to the endocycle during stage 6 [42,43]. We
260 found that in the developing egg chambers with germline mutations of *GlcT*, the patterning

261 of the surrounding follicle cells remained largely normal (Figure 6B). However, we observed
262 an abnormal accumulation of Dl protein in cytoplasmic vesicles of the mutant germline cells
263 (Figure 6C), indicating that there is a defect in Dl trafficking in *GlcT* mutant germline cells.
264 However, this defect is not sufficient to impact Dl-Notch signaling to a degree where follicle
265 cell development is adversely affected. Collectively, these observations suggest that the role
266 for GlcT in Notch signaling does not appear to be a universal mechanism across all
267 developmental contexts. Even in situations where this mechanism is involved, the extent to
268 which GlcT affects Dl-Notch signaling may vary in different developmental scenarios.

269

270 **Transient loss of *UGCG* in mouse small intestine causes reduced number of ISCs and**
271 **increased number of goblet cells**

272 As both the Notch signaling and the metabolic pathway of GSLs are conserved from
273 *Drosophila* to mammals, we asked whether this mechanism is conserved in the mouse small
274 intestine to regulate the proliferation and differentiation of ISCs. Notch is known to control
275 the absorptive versus secretory cell fate of mammalian intestinal progenitors as well, and the
276 inhibition of Notch signaling in the intestinal epithelium of mouse small intestine leads
277 excessive number of goblet cells [44,45]. However, unlike in *Drosophila*, Notch positively
278 regulates ISC self-renewal in mice. The inhibition of Notch causes ISC loss, and the excessive
279 activation of Notch promotes the proliferation of intestinal progenitor cells [45,46]. We
280 therefore performed conditional knockout of *UGCG*, which encodes the mammalian
281 glucosylceramide synthase, in the mouse small intestine and examined the consequences.

282

283 It has been previously reported that in the new born mice with intestine-specific knockout of
284 *UGCG*, the proliferation of enterocytes appeared largely normal. However, 3-4 days after
285 intestinal-specific knockout of UGCG in adult mice, epithelial phenotypes including epithelial
286 hyperproliferation, impaired lipid absorption and the detachment of enterocytes from the
287 basal lamina were observed, and these phenotypes are considered to be consequences of
288 gut barrier disruption [47]. To separate the primary from the secondary phenotypes, we

289 repeated the experiment by generating *UGCG*$^{flox/flox}$*; Vil-CreERT2* mice, and examined the
290 phenotype at 48h post tamoxifen administration, an early timepoint with a hope that the
291 secondary phenotypes have not yet developed.

292

293 Consistent with the previous findings, the conditional knockout mice showed a severe
294 diarrhea phenotype and died several days following tamoxifen induction. Interestingly, we
295 observed a few phenotypes at the 48h timepoint that was not observed before. We found
296 that in the mutant intestine, there was a marked increase in crypt depth accompanied by a
297 marked reduction in villus length (Supplementary Figure 3). In addition, an excess population
298 of goblet cells was observed, dispersed along the crypt-villus axis (Figure 7C, D). By
299 examining the expression of Olfm4, which is transcriptionally regulated by Notch in ISCs [48],
300 we found that the fluorescence intensity of Olfm4 staining was significantly reduced in *UGCG*
301 mutant ISCs (Figure 7A, B). It is unclear how the crypt-villus morphology phenotype is
302 developed in *UGCG* mutant epithelium, but the increased goblet cells and the reduced
303 expression level of Olfm4 are consistent with a Notch phenotype, suggesting a conserved
304 role for glucosylceramide synthase in modulating Notch signaling from *Drosophila* to
305 mammals.

306

307 **Discussion**

308 From an unbiased genetic screen on the right arm of chromosome II, here we have
309 pinpointed four mutant loci that cause an excessive EE phenotype in the intestinal
310 epithelium. Three of them encode known components of the Notch signaling (*mam*, *Gmer*,
311 and *O-fut1*), and the remaining one, *GlcT*, turns out to be a new Notch regulator as well. This
312 work further reinforces the notion that Notch as the key regulator of the secretory versus
313 absorptive cell fate decisions from ISCs, and reveals an evolutionarily conserved link between
314 GSL metabolism and Notch signaling in regulating intestinal homeostasis.

315

316 As *GlcT* encodes glucosylceramide synthase, which that catalyzes the formation of
317 glucosylceramide from ceramide, we further analyzed *egh* and *brn*, which encodes enzymes
318 for the subsequent sequential modifications of glucosylceramide by adding the second
319 (Mactosyl-) and third (GlcNAc-) glycosyl residues, respectively. We found that loss of *egh*, but
320 not *brn*, can give rise to a similar excessive EE phenotype. In addition, the phenotype caused
321 by *GlcT* can be suppressed by feeding with LacCer, which is analogous to MacCer. Collectively,
322 these observations demonstrate that the excessive EE phenotype caused by *GlcT* or *egh*
323 mutation is a result of MacCer deficiency.

324

325 GSLs constitute a specific category of glycolipids localized on the outer leaflet of eukaryotic
326 cell membranes, and studies have implicated their roles in regulating multiple cellular
327 signaling pathways by serving on the lipid raft to facilitate signaling transductions [49-52]. In
328 particular, there is an evolutionarily conserved phospholipid binding domain (C2 domain) on
329 the Notch ligand that is known to interacts with GSLs, and this interaction facilitates
330 ligand-receptor interactions and thereby promotes robust Notch signaling [53-55]. Our analyses
331 of *GlcT* mutant cells in the *Drosophila* midgut suggest that MacCer may represent a key
332 member of GSLs in facilitating Dl-Notch signaling transduction between intestinal stem cells
333 (ISCs) and their immediate progeny to steer binary cell fate decisions. To do so, MacCer may
334 help to modulate the endocytic trafficking of Dl, an event that is known to be essential for
335 Notch activation. We found that Dl on membrane of *GlcT* mutant ISCs tends be rapidly
336 endocytosed and the resultant endosomes appear to experience a delay in transition from
337 early endosome to late endosome. Prior genetic investigations have linked glycosphingolipids
338 synthesized by α4GT1 to the modulation of Dl ligand activity i*n vivo*. While the loss of α4GT1
339 does not overtly affect Dl-Notch signaling, it can exacerbate the wing phenotype of
340 haploinsufficient *Notch* mutants. Furthermore, the overexpression of α4GT1 has been shown
341 to counteract signaling and endocytosis dysfunctions of Dl caused by the inhibition of the E3
342 ligase Mib1 or Neur activity [50]. Therefore, the robust genetic results presented in this study
343 provide definitive evidence for a functional role of MacCer and its downstream derivatives in
344 regulating Notch signaling. Future structural studies focusing on the interactions between

345 GSLs and Dl should offer valuable insights into the role of GSLs in modulating Dl-Notch
346 interactions and membrane trafficking processes.

347

348 One intriguing observation from our study is the tissue-specific regulatory role of *GlcT* in
349 Notch signaling. Its loss in ISCs significantly impairs Notch signaling, leading to the formation
350 of EE tumors. However, when *GlcT* is lost in the germline cyst within the developing egg
351 chamber, it only modestly disrupts the endocytic trafficking of Dl, without conspicuous
352 effects on the differentiation and patterning of surrounding follicle cells. In the context of
353 imaginal discs, the loss of *GlcT* appears to have no discernible impact on Notch signaling
354 activity at all. This tissue-specific modulation of Notch signaling by *GlcT* suggests a potential
355 variability in membrane lipid composition across different cell types. Such variability could
356 render certain cells more susceptible to alterations in specific GSLs and their influence on
357 Dl-Notch signaling transduction, while others remain unaffected. As Dl trafficking in
358 *Drosophila* ISCs can be modulated by dietary lipid content, which impacts the duration and
359 level of Notch activation to control the production of EEs in newly enclosed flies [18], the
360 sensitivity of ISCs to specific GSL content may serve as a mechanism enabling ISCs to govern
361 the fate of their progeny based on nutrient content.

362

363 Taken together, our study identified MacCer/LacCer as a tissue-specific regulator of Dl-Notch
364 signaling by regulating the membrane localization and endocytic trafficking of Dl. As Notch
365 signaling has pleiotropic roles in many developmental processes, diseases and cancer, the
366 findings should contribute to our understanding of Notch signaling transduction and may
367 help to open up new approaches for developing prevention and treatments against human
368 diseases and cancer.

369

370

371 **ACKNOWLEDGEMENTS**

372 We thank Drs. Feng Yu and Sanduo Zheng for technical assistance, Drs. Dick Nassel,

Jan-Adrianus Veenstra, Zhaohui Wang, and the Developmental Studies Hybridoma Bank (DSHB) for antibodies, Drs. Sarah Bray, Steven Hou, Akiko Satoh, Tao Wang, the Bloomington Drosophila Stock Center (BDSC) and Vienna Drosophila Resource Center (VDRC) for fly stocks, and Dr. Sylvie Robine for the villin-Cre^{ERT2} mice. This work was supported by National Key Research and Development Program of China (2020YFA0803502 and 2017YFA0103602 to R.X.) from the Chinese Ministry of Science and Technology.

DECLARATION OFINTERESTS

The authors declare no competing interests.

MATERIALS AND METHODS

Drosophila Stocks and mice

Drosophila melanogaster stocks were maintained on standard cornmeal molasses food in a 25°C incubator. Flies for all experiments were maintained at a constant 25°C with 15–25 flies per vial and tossed onto new food every 2–3 days. *Drosophila* stocks used in this study: *hsflp, act-GAL4, UAS-GFP; FRT42B tub-GAL80; hsflp, act-GAL4, UAS-GFP; FRT42D tub-GAL80;* and *hsflp, Tub-GAL80, FRT19A; act-GAL4,UAS-GFP/Cyo* [56]; *hsflp; FRT42D, arm-lacZ/Cyo; esg-GAL4, UAS-GFP* [56]; *Su(H)GBE (NRE)-GAL4;* and *Dl-Gal4* [57]; *Su(H)GBE-lacZ* (NRE-lacZ, gift from Sarah Bray); *Glc^{EA30}*(generated in this study); *Glc^{E230}*(generated in this study); *GlcT$^{\Delta 8}$* [23]; *Tub-GAL80^{ts}* [58]; *UAS-GlcT* (generated in this study); *GlcT-RNAi* #1 (VDRC, id:44912); *GlcT-RNAi* #2 (VDRC, id:108064); *UAS-CDase* (gift from Tao Wang); *UAS-p35* (BDSC, #6298); *egh^{A}* (BDSC, #52353); *egh^{B}* (BDSC, #52354); *egh^{7}* (BDSC, #77889); *brn^{228}* (BDSC, #7392); *β4GalNAcTA-RNAi* (VDRC, id:4867); *α4GT1-RNAi* (VDRC, id:2608); *UAS-N^{intra}* [56]; *UAS-GFP-Rab5* (BDSC, #43336).

Mice used in this study include floxed *UGCG*, which was generated as previously described [47], and villin-CreERT2 [59]. All the research performance underwent strict ethical review and was approved by the Ethics Committee of the National Institute of Biological Sciences, Beijing. Mice were housed at the animal center in the National Institute of Biological Sciences in a Specific Pathogen Free (SPF) facility.

EMS Mutagenesis in *Drosophila*

403 3~5 day-old, isogenized y w; FRT42B(G13) males were subjected to a 10-hour starvation
404 period before being fed with EMS (30 mM in sucrose solution applied on filter papers)
405 overnight. Following recovery, these males were mated with y w; Sco/Cyo virgin females. In
406 the F1 offspring, y w; FRT42B */Cyo males were individually mated with several y w; Sco/Cyo
407 virgin females. The y w; FRT42B */Cyo males and virgin females in the F2 generation were
408 carefully selected and crossed with each other to establish balanced stocks for further
409 genetic studies. Altogether, around 10,000 stocks harboring lethal mutations were obtained
410 and screened.

411

412 **Deficiency Mapping**

413 The complete Bloomington Deficiency Kit for chromosome 2R
414 (https://bdsc.indiana.edu/stocks/df/dfkit-info.html) was used for initial mapping, which
415 helped to localize both the EA30 and E230 lethal mutations to a cytogenetic location
416 between 58A3 and 58F1. Subsequent mapping with additional deficiency lines encompassing
417 this region allowed the identification of two small deficiency lines, Df(2R)Exel7170 and
418 Df(2R)Excel6078, which failed to complement both mutations. This refinement narrowed the
419 critical region down to 58B2-58C1. There are 13 protein-coding genes within this region, and
420 genomic sequencing data indicated that both lines carried missense mutations on the *GlcT*
421 gene, as described in the text.

422

423 **Genomic Sequencing and Analysis Method**

424 As all mutants exhibited lethality in the adult stage, homozygous larvae were selected using a
425 green balancer, and the extracted genomic DNAs were sequenced at BGI Genomics using a
426 library with an insert size of ≤800bp. The sequencing platform employed was the HiSeq 2000.
427 For sequence analysis, all mutants were compared to a reference genome. Subsequently,
428 sequencing reads were assigned to each allele based on heterozygote SNPs retained using a
429 custom Perl script. The candidate heterozygous sites were annotated using snpEff.

430

431 **Mosaic Analysis with a Repressible Cell Marker (MARCM) Analysis**

432 To generate MARCM clones [60], flies of the desired genotype were raised and maintained at
433 25°C until they reached 7 days of age. Subsequently, they were subjected to a 60-minute
434 heat shock in a water bath at 37°C. Following the heat shock, the flies were fed with standard
435 food supplemented with yeast paste and this feeding regimen was repeated every 2 days
436 before the flies were dissected for further analysis.

437

438 **GAL4/GAL80^{ts} System**

439 The GAL4/UAS and GAL80ts systems were utilized as previously described [58,61]. To inhibit the
440 GAL4 system, the crosses were sustained at 18°C when employing temperature-sensitive
441 GAL4-mediated RNAi or gene overexpression. Subsequently, F1 adult flies with the correct
442 genotype were transitioned to 29°C to activate the GAL4 system, thereby triggering RNAi or
443 gene overexpression.

444

445 **Tamoxifen Treatment in Mice**

446 Cre recombinase activity was induced via intraperitoneal injection of 2 mg tamoxifen
447 (Sigma-Aldrich, T5648), and tissues were collected 48 hours post-injection. Cre-negative
448 littermates served as controls.

449

450 **Immunofluorescent Staining and Imaging**

451 Adult female midguts were dissected in PBS and fixed for 30 minutes at room temperature in
452 4% paraformaldehyde. The fixed tissues were then dehydrated in methanol for 5 minutes
453 followed by rehydration in a PBT solution (PBS containing 0.1% Triton X-100). The tissues
454 underwent four washes with 0.1% Triton in 1×PBS (PBST) and were subsequently incubated
455 with PBST and primary antibodies overnight at 4°C. After another round of washing, the
456 samples were incubated for 2 hours with secondary antibodies in PBST. Finally, the samples
457 were stained with DAPI for visualization of nuclei.

458 Mouse small intestine was dissected out and gently flushed with cold 1× PBS to remove fecal
459 content, and fixed overnight at 4°C in 4% paraformaldehyde (PFA) prepared in 1× PBS. The
460 tissue was then incubated in a 30% sucrose solution at 4°C for 24 hours, and embedded in
461 OCT (Tissue-Tek) before frozen. Frozen sections of 15 μm thickness were prepared for further
462 analysis. For immunostaining, tissue sections were permeabilized with 1% Triton X-100

463 (Sigma-Aldrich) in PBS for 1 hour at room temperature (RT), followed by blocking with a
464 solution containing 0.2% Triton X-100, 1% bovine serum albumin (BSA), and 3% goat serum
465 in PBS for 1 hour at RT before antibody staining. The sections were mounted in Vectashield
466 mounting media with DAPI (Vector Laboratories) for imaging.

467 Primary antibodies used in this study: mouse anti-Pros (DSHB #MR1A; 1:300); mouse anti-Dl
468 (DSHB Cat#C594.9B; RRID:AB_528194; 1:300); rabbit anti-AstC (gift from Dr. Dick Nassel;
469 1:300); rabbit anti-Tk (gift from Dr. Jan-Adrianus Veenstra; 1:300); Rabbit anti-pH3 (CST Cat#
470 9701; RRID:AB_331535; 1:500); mouse monoclonal anti-β-galactosidase (DSHB, #40-1a; 1:30);
471 mouse anti-Cut (DSHB, #2B10; 1:20); mouse anti-Rab7 (DSHB, 1:300); rabbit anti-pERK (CST,
472 1:200); rabbit anti-STAT92E (gift from Dr. Zhaohui Wang, 1:300); rabbit anti-DCP-1 (CST
473 Cat#9578S; 1:300); mouse monoclonal anti-EYA (DSHB, #10H6; 1:300); rabbit monoclonal
474 anti-GFP (Invitrogen Cat#G10362; 1:300). Secondary antibodies used in this study include
475 Alexa Fluor 568- or Cy5-conjugated goat anti-rabbit, anti-mouse IgGs (Molecular Probes,
476 A11034-A11036, A10524; 1:300). For nuclei staining, DAPI (Sigma-Aldrich, 1 μg/ml) was used.
477 The preparations were mounted in 70% glycerol, and the slides were stored at -20°C. Imaging
478 was conducted using a Leica SP8 confocal microscope. All captured images were processed
479 and compiled using Adobe Photoshop and Illustrator.

480

481 **LacCer Treatment**

482 The 2-3 days old female flies of the specified genotype were moved to fresh food layered
483 with a filter paper soaked in a 5% sucrose solution containing 20 μM of LacCer
484 (Sigma-Aldrich CAS#4682-48-8) and this transfer was repeated daily before dissection and
485 analysis.

486

487 **Antibody Uptake Assay**

488 The anti-Dl antibody Uptake assay was conducted following a previously described protocol
489 [40]. In brief, the *Drosophila* gut was dissected and placed in fresh medium containing
490 anti-Delta. The dissecting dish was then placed in a humidified box and incubated at 25 °C for
491 the necessary duration. Subsequently, the medium containing the antibody was removed,
492 and a single wash with Schneider's *Drosophila* medium was carried out. The midgut was then
493 fixed directly in the dissecting dish for 20 minutes under a chemical fume hood by adding 1
494 ml of fixative. Following this, samples underwent three washes with PBT and were then

incubated for 60 minutes with fluorescently labeled anti-mouse secondary antibodies in PBT on a rotating platform. After another three washes with PBT, the samples were mounted in 50% glycerol in PBS for analysis under microscopy.

Fluorescence Intensity Statistics

The Image J software (downloaded from https://imagej.nih.gov/ij/) was utilized to measure the fluorescence intensity of the captured images. The corrected fluorescence intensity is determined as the average fluorescence intensity of each cell's nuclear region minus the average background fluorescence intensity.

Statistical analysis

All quantifications were presented in the form of mean ± SEM. GraphPad Prism 5 software (GraphPad Software Inc.) was used to calculate p-values using an unpaired Student's t-test. The number of intestines used for calculations was labeled on the figures or in the related figure legends.

REFERENCES

1. Bray, S.J. (2006). Notch signalling: a simple pathway becomes complex. Nat Rev Mol Cell Biol *7*, 678-689. 10.1038/nrm2009.
2. Kopan, R., and Ilagan, M.X. (2009). The canonical Notch signaling pathway: unfolding the activation mechanism. Cell *137*, 216-233. 10.1016/j.cell.2009.03.045.
3. Artavanis-Tsakonas, S., Rand, M.D., and Lake, R.J. (1999). Notch signaling: cell fate control and signal integration in development. Science *284*, 770-776.
4. Penton, A.L., Leonard, L.D., and Spinner, N.B. (2012). Notch signaling in human development and disease. Semin Cell Dev Biol *23*, 450-457. 10.1016/j.semcdb.2012.01.010.
5. Bolos, V., Grego-Bessa, J., and de la Pompa, J.L. (2007). Notch signaling in development and cancer. Endocr Rev *28*, 339-363. 10.1210/er.2006-0046.
6. Boumard, B., and Bardin, A.J. (2021). An amuse-bouche of stem cell regulation: Underlying principles and mechanisms from adult Drosophila intestinal stem cells. Curr Opin Cell Biol *73*, 58-68. 10.1016/j.ceb.2021.05.007.
7. Koch, U., Lehal, R., and Radtke, F. (2013). Stem cells living with a Notch. Development *140*, 689-704. 10.1242/dev.080614.

527 8. Ohlstein, B., and Spradling, A. (2007). Multipotent Drosophila intestinal stem cells specify
528 daughter cell fates by differential notch signaling. Science *315*, 988-992. 315/5814/988
529 [pii10.1126/science.1136606 [doi].
530 9. Ohlstein, B., and Spradling, A. (2006). The adult Drosophila posterior midgut is maintained by
531 pluripotent stem cells. Nature *439*, 470-474. nature04333 [pii]10.1038/nature04333 [doi].
532 10. Chen, J., Xu, N., Wang, C., Huang, P., Huang, H., Jin, Z., Yu, Z., Cai, T., Jiao, R., and Xi, R. (2018).
533 Transient Scute activation via a self-stimulatory loop directs enteroendocrine cell pair
534 specification from self-renewing intestinal stem cells. Nat Cell Biol *20*, 152-161.
535 10.1038/s41556-017-0020-0.
536 11. Micchelli, C.A., and Perrimon, N. (2006). Evidence that stem cells reside in the adult
537 Drosophila midgut epithelium. Nature *439*, 475-479. nature04371 [pii]10.1038/nature04371
538 [doi].
539 12. Guo, Z., and Ohlstein, B. (2015). Stem cell regulation. Bidirectional Notch signaling regulates
540 Drosophila intestinal stem cell multipotency. Science *350*. 10.1126/science.aab0988.
541 13. Henrique, D., and Schweisguth, F. (2019). Mechanisms of Notch signaling: a simple logic
542 deployed in time and space. Development *146*. 10.1242/dev.172148.
543 14. Yin, C., and Xi, R. (2018). A Phyllopod-Mediated Feedback Loop Promotes Intestinal Stem Cell
544 Enteroendocrine Commitment in Drosophila. Stem Cell Reports *10*, 43-57.
545 10.1016/j.stemcr.2017.11.014.
546 15. Wang, C., Guo, X., Dou, K., Chen, H., and Xi, R. (2015). Ttk69 acts as a master repressor of
547 enteroendocrine cell specification in Drosophila intestinal stem cell lineages. Development
548 *142*, 3321-3331. 10.1242/dev.123208.
549 16. Guo, X., Zhang, Y., Huang, H., and Xi, R. (2022). A hierarchical transcription factor cascade
550 regulates enteroendocrine cell diversity and plasticity in Drosophila. Nat Commun *13*, 6525.
551 10.1038/s41467-022-34270-0.
552 17. de Navascues, J., Perdigoto, C.N., Bian, Y., Schneider, M.H., Bardin, A.J., Martinez-Arias, A.,
553 and Simons, B.D. (2012). Drosophila midgut homeostasis involves neutral competition
554 between symmetrically dividing intestinal stem cells. EMBO J *31*, 2473-2485.
555 10.1038/emboj.2012.106.
556 18. Obniski, R., Sieber, M., and Spradling, A.C. (2018). Dietary Lipids Modulate Notch Signaling
557 and Influence Adult Intestinal Development and Metabolism in Drosophila. Dev Cell *47*,
558 98-111 e115. 10.1016/j.devcel.2018.08.013.
559 19. Perdigoto, C.N., Schweisguth, F., and Bardin, A.J. (2011). Distinct levels of Notch activity for
560 commitment and terminal differentiation of stem cells in the adult fly intestine. Development
561 *138*, 4585-4595. dev.065292 [pii]10.1242/dev.065292.
562 20. Ayukawa, T., Matsumoto, K., Ishikawa, H.O., Ishio, A., Yamakawa, T., Aoyama, N., Suzuki, T.,
563 and Matsuno, K. (2012). Rescue of Notch signaling in cells incapable of GDP-L-fucose
564 synthesis by gap junction transfer of GDP-L-fucose in Drosophila. Proc Natl Acad Sci U S A *109*,
565 15318-15323. 10.1073/pnas.1202369109.
566 21. Petcherski, A.G., and Kimble, J. (2000). Mastermind is a putative activator for Notch. Curr Biol
567 *10*, R471-473. 10.1016/s0960-9822(00)00577-7.
568 22. Sasamura, T., Ishikawa, H.O., Sasaki, N., Higashi, S., Kanai, M., Nakao, S., Ayukawa, T., Aigaki, T.,
569 Noda, K., Miyoshi, E., et al. (2007). The O-fucosyltransferase O-fut1 is an extracellular

570 component that is essential for the constitutive endocytic trafficking of Notch in Drosophila.
571 Development *134*, 1347-1356. 10.1242/dev.02811.
572 23. Satoh, T., Inagaki, T., Liu, Z., Watanabe, R., and Satoh, A.K. (2013). GPI biosynthesis is essential
573 for rhodopsin sorting at the trans-Golgi network in Drosophila photoreceptors. Development
574 *140*, 385-394. 10.1242/dev.083683.
575 24. Selzner, M., Bielawska, A., Morse, M.A., Rudiger, H.A., Sindram, D., Hannun, Y.A., and Clavien,
576 P.A. (2001). Induction of apoptotic cell death and prevention of tumor growth by ceramide
577 analogues in metastatic human colon cancer. Cancer Res *61*, 1233-1240.
578 25. Ryoo, H.D., Gorenc, T., and Steller, H. (2004). Apoptotic cells can induce compensatory cell
579 proliferation through the JNK and the Wingless signaling pathways. Dev Cell *7*, 491-501.
580 10.1016/j.devcel.2004.08.019.
581 26. Wandall, H.H., Pizette, S., Pedersen, J.W., Eichert, H., Levery, S.B., Mandel, U., Cohen, S.M.,
582 and Clausen, H. (2005). Egghead and brainiac are essential for glycosphingolipid biosynthesis
583 in vivo. J Biol Chem *280*, 4858-4863. 10.1074/jbc.C400571200.
584 27. Muller, R., Altmann, F., Zhou, D., and Hennet, T. (2002). The Drosophila melanogaster brainiac
585 protein is a glycolipid-specific beta 1,3N-acetylglucosaminyltransferase. J Biol Chem *277*,
586 32417-32420. 10.1074/jbc.C200381200.
587 28. Stolz, A., Haines, N., Pich, A., Irvine, K.D., Hokke, C.H., Deelder, A.M., Gerardy-Schahn, R.,
588 Wuhrer, M., and Bakker, H. (2008). Distinct contributions of beta 4GalNAcTA and beta
589 4GalNAcTB to Drosophila glycosphingolipid biosynthesis. Glycoconj J *25*, 167-175.
590 10.1007/s10719-007-9069-5.
591 29. Chen, Y.W., Pedersen, J.W., Wandall, H.H., Levery, S.B., Pizette, S., Clausen, H., and Cohen, S.M.
592 (2007). Glycosphingolipids with extended sugar chain have specialized functions in
593 development and behavior of Drosophila. Dev Biol *306*, 736-749.
594 10.1016/j.ydbio.2007.04.013.
595 30. Xu, N., Wang, S.Q., Tan, D., Gao, Y., Lin, G., and Xi, R. (2011). EGFR, Wingless and JAK/STAT
596 signaling cooperatively maintain Drosophila intestinal stem cells. Dev Biol *354*, 31-43.
597 S0012-1606(11)00182-5 [pii]10.1016/j.ydbio.2011.03.018 [doi].
598 31. Jiang, H., Patel, P.H., Kohlmaier, A., Grenley, M.O., McEwen, D.G., and Edgar, B.A. (2009).
599 Cytokine/Jak/Stat signaling mediates regeneration and homeostasis in the Drosophila midgut.
600 Cell *137*, 1343-1355. S0092-8674(09)00571-6 [pii]10.1016/j.cell.2009.05.014 [doi].
601 32. Ohlstein, B., and Spradling, A. (2007). Multipotent Drosophila intestinal stem cells specify
602 daughter cell fates by differential notch signaling. Science *315*, 988-992.
603 33. Guo, Z., and Ohlstein, B. (2015). Bidirectional Notch signaling regulates Drosophila intestinal
604 stem cell multipotency. Science *350*, aab0988.
605 34. Jiang, H., Grenley, M.O., Bravo, M.J., Blumhagen, R.Z., and Edgar, B.A. (2011).
606 EGFR/Ras/MAPK signaling mediates adult midgut epithelial homeostasis and regeneration in
607 Drosophila. Cell Stem Cell *8*, 84-95.
608 35. Patel, P.H., Dutta, D., and Edgar, B.A. (2015). Niche appropriation by Drosophila intestinal
609 stem cell tumours. Nat Cell Biol *17*, 1182-1192. 10.1038/ncb3214.
610 36. Beehler-Evans, R., and Micchelli, C.A. (2015). Generation of enteroendocrine cell diversity in
611 midgut stem cell lineages. Development *142*, 654-664. 10.1242/dev.114959.
612 37. Bray, S.J., and Gomez-Lamarca, M. (2018). Notch after cleavage. Current opinion in cell
613 biology *51*, 103-109.

614 38. Yamamoto, S., Charng, W.L., and Bellen, H.J. (2010). Endocytosis and intracellular trafficking
615 of Notch and its ligands. Curr Top Dev Biol *92*, 165-200. 10.1016/S0070-2153(10)92005-X.
616 39. Simons, K., and Toomre, D. (2000). Lipid rafts and signal transduction. Nat Rev Mol Cell Biol *1*,
617 31-39. 10.1038/35036052.
618 40. Couturier, L., and Schweisguth, F. (2014). Antibody uptake assay and in vivo imaging to study
619 intracellular trafficking of Notch and Delta in Drosophila. Methods Mol Biol *1187*, 79-86.
620 10.1007/978-1-4939-1139-4_6.
621 41. Micchelli, C.A., Rulifson, E.J., and Blair, S.S. (1997). The function and regulation of cut
622 expression on the wing margin of Drosophila: Notch, Wingless and a dominant negative role
623 for Delta and Serrate. Development *124*, 1485-1495.
624 42. Deng, W.-M., Althauser, C., and Ruohola-Baker, H. (2001). Notch-Delta signaling induces a
625 transition from mitotic cell cycle to endocycle in Drosophila follicle cells.
626 43. López-Schier, H., and Johnston, D.S. (2001). Delta signaling from the germ line controls the
627 proliferation and differentiation of the somatic follicle cells during Drosophila oogenesis.
628 Genes & development *15*, 1393-1405.
629 44. van Es, J.H., van Gijn, M.E., Riccio, O., van den Born, M., Vooijs, M., Begthel, H., Cozijnsen, M.,
630 Robine, S., Winton, D.J., Radtke, F., and Clevers, H. (2005). Notch/gamma-secretase inhibition
631 turns proliferative cells in intestinal crypts and adenomas into goblet cells. Nature *435*,
632 959-963.
633 45. Riccio, O., van Gijn, M.E., Bezdek, A.C., Pellegrinet, L., van Es, J.H., Zimber-Strobl, U., Strobl,
634 L.J., Honjo, T., Clevers, H., and Radtke, F. (2008). Loss of intestinal crypt progenitor cells owing
635 to inactivation of both Notch1 and Notch2 is accompanied by derepression of CDK inhibitors
636 p27Kip1 and p57Kip2. EMBO Rep *9*, 377-383. 10.1038/embor.2008.7.
637 46. Fre, S., Huyghe, M., Mourikis, P., Robine, S., Louvard, D., and Artavanis-Tsakonas, S. (2005).
638 Notch signals control the fate of immature progenitor cells in the intestine. Nature *435*,
639 964-968.
640 47. Jennemann, R., Kaden, S., Sandhoff, R., Nordstrom, V., Wang, S., Volz, M., Robine, S., Amen,
641 N., Rothermel, U., Wiegandt, H., and Grone, H.J. (2012). Glycosphingolipids are essential for
642 intestinal endocytic function. J Biol Chem *287*, 32598-32616. 10.1074/jbc.M112.371005.
643 48. VanDussen, K.L., Carulli, A.J., Keeley, T.M., Patel, S.R., Puthoff, B.J., Magness, S.T., Tran, I.T.,
644 Maillard, I., Siebel, C., Kolterud, A., et al. (2012). Notch signaling modulates proliferation and
645 differentiation of intestinal crypt base columnar stem cells. Development *139*, 488-497.
646 10.1242/dev.070763.
647 49. Coskun, U., Grzybek, M., Drechsel, D., and Simons, K. (2011). Regulation of human EGF
648 receptor by lipids. Proc Natl Acad Sci U S A *108*, 9044-9048. 10.1073/pnas.1105666108.
649 50. Hamel, S., Fantini, J., and Schweisguth, F. (2010). Notch ligand activity is modulated by
650 glycosphingolipid membrane composition in Drosophila melanogaster. J Cell Biol *188*,
651 581-594. 10.1083/jcb.200907116.
652 51. Ideo, H., Seko, A., Ishizuka, I., and Yamashita, K. (2003). The N-terminal carbohydrate
653 recognition domain of galectin-8 recognizes specific glycosphingolipids with high affinity.
654 Glycobiology *13*, 713-723. 10.1093/glycob/cwg094.
655 52. Park, S.Y., Kwak, C.Y., Shayman, J.A., and Kim, J.H. (2012). Globoside promotes activation of
656 ERK by interaction with the epidermal growth factor receptor. Biochim Biophys Acta *1820*,
657 1141-1148. 10.1016/j.bbagen.2012.04.008.

658 53. Suckling, R.J., Korona, B., Whiteman, P., Chillakuri, C., Holt, L., Handford, P.A., and Lea, S.M.
659 (2017). Structural and functional dissection of the interplay between lipid and Notch binding
660 by human Notch ligands. EMBO J *36*, 2204-2215. 10.15252/embj.201796632.
661 54. Martins, T., Meng, Y., Korona, B., Suckling, R., Johnson, S., Handford, P.A., Lea, S.M., and Bray,
662 S.J. (2021). The conserved C2 phospholipid-binding domain in Delta contributes to robust
663 Notch signalling. EMBO Rep *22*, e52729. 10.15252/embr.202152729.
664 55. Chillakuri, C.R., Sheppard, D., Ilagan, M.X., Holt, L.R., Abbott, F., Liang, S., Kopan, R., Handford,
665 P.A., and Lea, S.M. (2013). Structural analysis uncovers lipid-binding properties of Notch
666 ligands. Cell Rep *5*, 861-867. 10.1016/j.celrep.2013.10.029.
667 56. Lin, G., Xu, N., and Xi, R. (2008). Paracrine Wingless signalling controls self-renewal of
668 Drosophila intestinal stem cells. Nature *455*, 1119-1123. nature07329
669 [pii]10.1038/nature07329 [doi].
670 57. Zeng, X., Chauhan, C., and Hou, S.X. (2010). Characterization of midgut stem cell- and
671 enteroblast-specific Gal4 lines in drosophila. Genesis *48*, 607-611. 10.1002/dvg.20661 [doi].
672 58. McGuire, S.E., Mao, Z., and Davis, R.L. (2004). Spatiotemporal gene expression targeting with
673 the TARGET and gene-switch systems in Drosophila. Sci STKE *2004*, pl6.
674 59. el Marjou, F., Janssen, K.P., Chang, B.H., Li, M., Hindie, V., Chan, L., Louvard, D., Chambon, P.,
675 Metzger, D., and Robine, S. (2004). Tissue-specific and inducible Cre-mediated recombination
676 in the gut epithelium. Genesis *39*, 186-193. 10.1002/gene.20042.
677 60. Lee, T., and Luo, L. (1999). Mosaic analysis with a repressible cell marker for studies of gene
678 function in neuronal morphogenesis. Neuron *22*, 451-461. S0896-6273(00)80701-1 [pii].
679 61. Brand, A.H., and Perrimon, N. (1993). Targeted gene expression as a means of altering cell
680 fates and generating dominant phenotypes. Development *118*, 401-415.

681

682 **Figure legends**

683 **Figure 1. A mosaic genetic screen identifies *GlcT* as a tumor suppressor in adult *Drosophila***
684 **midgut**

685 (A) A diagram showing lineage hierarchy of intestinal stem cells (ISCs) in the *Drosophila*
686 intestine. Abbreviations: EB, enteroblast; EEP, enteroendocrine cell; EC, enterocyte; EE,
687 enteroendocrine cell. (B-D) Compared to control clones (green), the *EA30* and *E230* clones
688 induced at day 5 are larger and contain a higher number of *Pros*$^{+}$ cells within each clone. *GlcT*
689 null allele (*GlcT*$^{\Delta 8}$) mutant clones exhibit a similar phenotype. (E-F) Expression of *UAS-GlcT* in
690 *EA30* or *E230* mutant clones rescues the tumor phenotype. (G-J) Depletion of *GlcT* in
691 progenitor cells using RNAi with *esg-GAL4*^{ts} leads to ISC proliferation (G-H, stained with
692 Phospho-Histone 3) and excessive EEC generation in the midgut (I-J). For G-J, flies were
693 shifted to 29°C for 14 days. Error bars represent the mean ± SEM, with p-values indicated in
694 the figure (two-tailed Student's t-test). Scale bars: 25 µm.

695

696 **Figure 2. Genetic analysis of the components of the GSL synthesis pathway reveals specific**
697 **tumor-suppressive activity for *egh*, in addition to *GlcT***

698 (A) A diagram illustrating a portion of the metabolic pathways of glycosphingolipids (GSLs)
699 synthesized from ceramide, highlighting the key enzymes involved at each step. (B) *GlcT*$^{\Delta 8}$
700 mutant clones without or with co-expression of *p35* or *CDase* stained with anti-DCP-1 or
701 anti-Pros, as indicated. Clones were examined at day 7-10 after clone induction. (C-D)
702 Quantitative analysis of the percentage of Pros^{+} cells in clones of specified genotypes. (E)
703 Genetic analysis of the key enzymes in the GSL synthesis pathway. Note that *egh* mutant
704 clones (*egh*^{A}, *egh*^{B}, or *egh*^{7}) exhibited a phenotype of increased EEs similar to that observed
705 in *GlcT* mutant clones, but *Brn*^{228}, *β4GalNAcTA-IR*, and *α4GT1-IR* clones did not. (F, G)
706 Quantitative analysis of cell number (F) and the percentage of Pros^{+} cells (G) in clones of
707 specified genotypes. For E-G, clones were examined at day 7 after clone induction. Error bars
708 represent the mean ± SEM, with p-values indicated in the figure (two-tailed Student's t-test).
709 Scale bars: 25 µm.

710

711 **Figure 3. The EE tumor phenotype is a result of MacCer deficiency**

712 (A) A diagram showing the major compartments along the length of the *Drosophila* midgut,
713 including the anterior (yellow), middle (Region 3, R3, green), and posterior midgut (blue).
714 (B-C) Feeding *GlcT* mutant flies with LacCer alleviated the overgrowth and excessive EE
715 phenotype, which was observed in clones of both the anterior and posterior midgut. Note
716 that the suppressive effect was more pronounced in the anterior midgut compared to the
717 posterior midgut. Error bars represent the mean ± SEM, with p-values indicated in the figure
718 (two-tailed Student's t-test). Scale bar: 25 µm.

719

720 **Figure 4. Loss of *GlcT* leads to reduced activation of Notch signaling in ISC progenies**

721 (A-B) The expression of *NRE-lacZ*, the Notch activity reporter, in *GlcT* mutant clones. Note
722 that the fluorescence intensity of LacZ was significantly reduced within *GlcT* mutant clones
723 compared to the cells outside of the clone. (C) *GlcT* mutant clones in the posterior (R5)
724 region of the *Drosophila* midgut stained with anti-Tk (left) or anti-AstC (right). The two EE
725 subtypes at R5 region are normally present in a 1:1 ratio. Note that $AstC^+$ EEs, but not TK^+ EEs,
726 were present in *GlcT* mutant clones. (D) The effect of forced activation of Notch in *GlcT*
727 mutant clones by expressing N^{intra}. Error bars represent the mean ± SEM, with p-values
728 indicated in the figure (two-tailed Student's t-test). Scale bars: 25 µm.

729

730 **Figure 5. *GlcT* regulates the endocytic trafficking of Delta**

731 (A-B) Anti-Pros staining in flies carrying *GlcT-IR* driven by Dl^{ts} and NRE^{ts} respectively. Flies
732 were shifted to 29°C for 14 days before analysis. (C) In a 3-hour Dl antibody uptake assay
733 performed in the *Drosophila* midgut, Dl in ISCs of *GlcT* mutant clones (green box) showed
734 reduced membrane localization and increased intracellular fluorescence compared to that in
735 ISCs of control clones (see the enlarged inset boxes). (D, F) ISCs in esg^{ts}>*GlcT-RNAi* flies
736 exhibited increased accumulation of Dl in early endosomes ($Rab5^+$, with co-localization

737 indicated by yellow arrows). (E-F) The percentage of Dl^{+} late endosomes (Rab7^{+}) was largely
738 unchanged. For D-F, flies were shifted to 29°C for 10 days before analysis. Co-localization
739 analysis was performed using the intensity-based quantification feature in Leica Application
740 Suite X (LAS X) software, with the Overlap Coefficient (ranging from 0 to 1) employed to
741 quantify co-localization (1 indicating perfect co-localization and 0 indicating no
742 co-localization). Error bars represent the mean ± SEM, with p-values indicated in the figure
743 (two-tailed Student's t-test). Scale bar: 25 µm, unless otherwise noted.

744

745 **Figure 6. *GlcT* shows tissue specificity in regulating Notch signaling activity**

746 (A) The expression of Cut in a *GlcT* mutant clone (green area) in wing disc spanning the
747 dorsal-ventral boundary. (B) The expression of EYA in *GlcT* mutant follicle cell clones
748 (non-green areas). Note that there was no obvious difference in the level of EYA expression
749 inside and outside of the clones. (C) Punctate accumulation of Dl was observed in *GlcT*
750 mutant germ cell clones (non-green area, indicated by arrows in the enlarged inset), but not
751 in the germline of a wild-type developing egg chamber (see enlarged inset with the dashed
752 yellow line). Scale bars: 25 µm.

753

754 **Figure 7. Transient loss of *UGCG* in mouse small intestine causes reduced number of ISCs**
755 **and increased number of goblet cells**

756 (A-B) The expression of the Notch target gene O*lfm4* was downregulated in *villin-Cre^{ERT2}*,
757 *UGCG$^{flox/flox}$* mice 48 hours post-induction (n=3). The *CKO* mice displayed shorter villi (above
758 the dotted line) and elongated crypts (below the dotted line). (C-D) The number of Muc2^{+}
759 goblet cells was significantly increased in the *CKO* mice. (E) A schematic model for the role of
760 MacCer in regulating the Notch signaling pathway. In signaling-sending cells, mutations in
761 *GlcT* result in the loss of the downstream metabolite MacCer, leading to a rapid endocytosis
762 of the membrane Dl and an accumulation of Dl in early endosomes. This causes a reduced
763 level of Notch signaling activation in signaling-receiving cells. Error bars represent the mean
764 ± SEM, with p-values indicated in the figure (two-tailed Student's t-test). Scale bars: 100 µm.

765

766 **Supplementary Figure 1. Cross scheme for the mosaic genetic screen on the 2R chromosome.**

767 (A) A schematic illustrating the principles of FLPase-induced mitotic recombination for
768 generating homozygous mutant cells in heterozygous animals. (B) The cross scheme and
769 workflow for the forward genetic mosaic screen conducted in this study. Abbreviation: EMS,
770 ethyl methanesulfonate.

771

772 **Supplementary Figure 2. The EGFR/Ras/MAPK and JAK/STAT signaling activities in *GlcT***
773 **mutant clones.**

774 *GlcT* mutant clones stained with pERK (red, upper panels), a direct indicator of
775 EGFR/Ras/MAPK signaling activity, and STAT92E (red, lower panels), whose nuclear
776 localization is indicative of JAK/STAT signaling activity. Note that pERK was not significantly
777 increased in *GlcT* mutant cells compared to normal cells outside of the clones, and STAT92E
778 activity was also not obviously altered in *GlcT* mutant cells compared to normal cells outside
779 the clones. Scale bar: 25 µm.

780

781 **Supplementary Figure 3. The Crypt-Villus morphology in *UGCG* CKO mice. The duodenal**
782 **structure exhibits significant abnormalities in *CKO* mice**

783 Small intestine (duodenum) from control and *villin-creERT2, UGCG*$^{flox/flox}$ mice stained with
784 K20, which marks enterocytes and goblet cells, and Ki67, which marks proliferative cells.
785 Note that the mutant intestine has shortened villi and elongated crypts. Dotted lines indicate
786 the boundary between the crypt and the villus. Samples were collected at 48h after
787 tamoxifen injection. Scale bar: 100 µm.